PNAS
www.pnas.org

Supplementary Information for

New insights into ice multiplication using remote-sensing observations of slightly supercooled mixed-phase clouds in the Arctic

Edward P. Luke, Fan Yang, Pavlos Kollias, Andrew M. Vogelmann, and Maximilian Maahn

Edward P. Luke and Fan Yang.
E-mail: eluke@bnl.gov, fanyang@bnl.gov

This PDF file includes:

Other supplementary materials for this manuscript include the following:

Movie S1

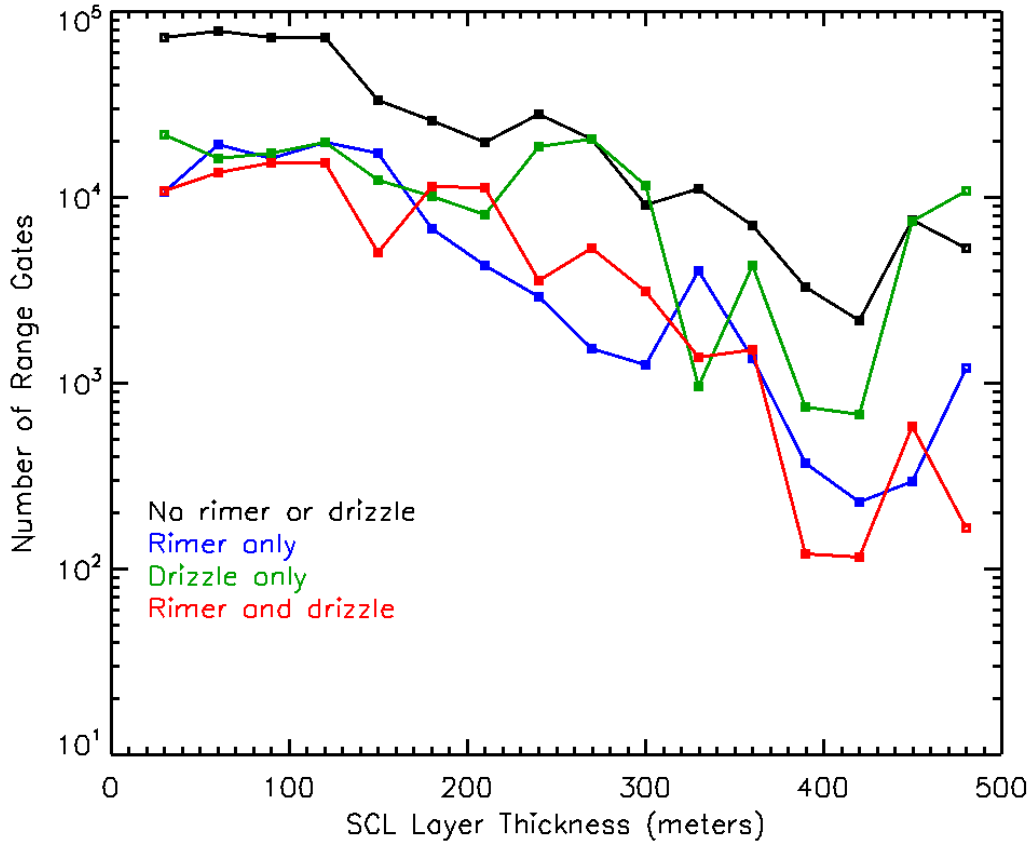

Fig. S1. Frequency of occurrence of range gates versus thickness of the supercooled liquid layer to which they belong, partitioned by the class of their local neighborhood. 95% of range gates in each subgroup are within clouds with thicknesses of about 330 m or less.

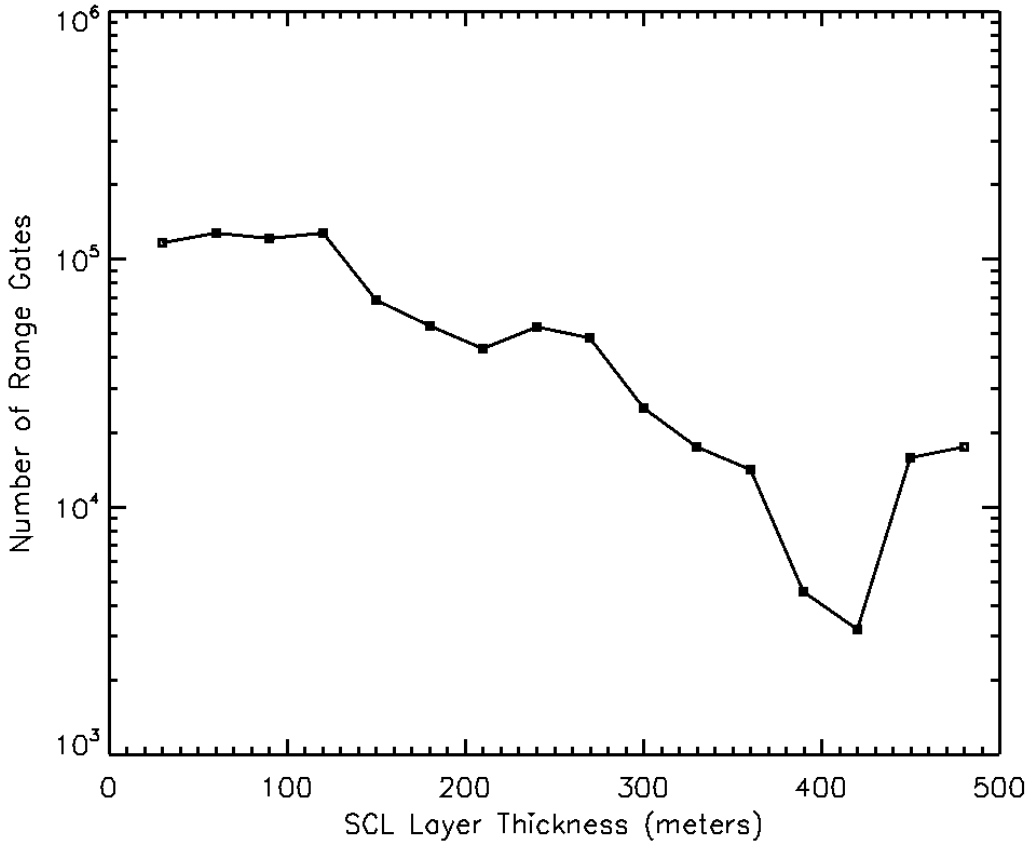

Fig. S2. Frequency of occurrence of the total number of range gates versus thickness of the supercooled liquid layer to which they belong. 95% of the range gates are found in clouds with thickness < 360 m.

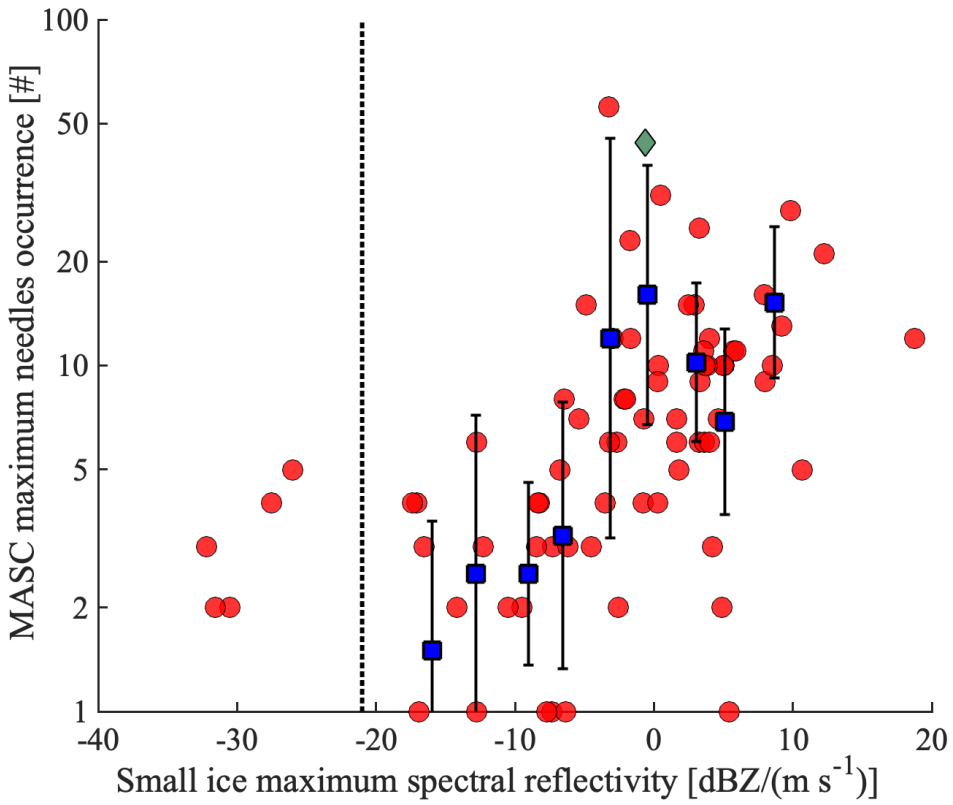

Fig. S3. For the 7-mo period during which operation of the surface-based multiangle snowflake camera (MASC) coincided with our study, the red points show the maxima in camera-observed needle occurrences within $\pm$25 min of a given sounding versus the corresponding peak spectral radar reflectivity value used to derive secondary ice multiplication based on our method. The blue squares with black line segments show the mean and standard deviation of needle occurrences within a spectral reflectivity bin 3 dBZ s m^{-1} wide. The vertical black dotted line depicts the threshold between "background" small ice and secondary ice multiplication detections. The green diamond corresponds to the May 11, 2019 case presented in the manuscript.

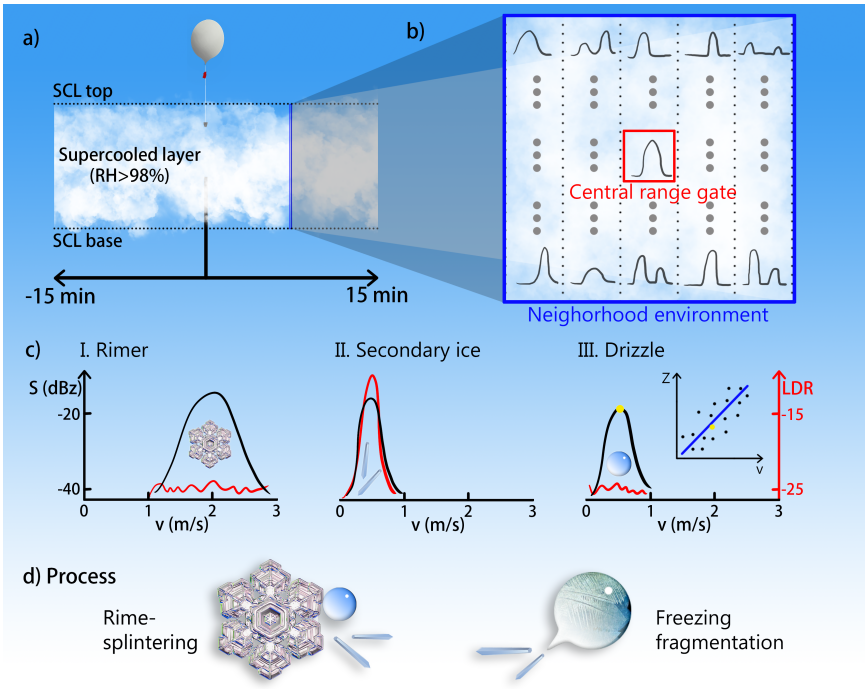

Fig. S4. Schematic diagram of the research methodology used to investigate the occurrence and conditions of secondary ice production events in slightly supercooled liquid cloud using radar Doppler spectra. a) The radar Doppler spectra used for this study are limited to those occurring within 15 minutes and 4 lateral km of a balloon sounding, where relative humidity is above 98% and temperature is between 0 and -10^{o}C. b) Any Doppler spectrum — labeled as central range gate — is assumed to be related to other Doppler spectra from its neighborhood environmental region, defined as all surrounding gates within a window of 2 minutes and a vertical extent of 200 m. Each range gate is a cylindrical sampling volume of about 380 m^{3}, measuring 4 m in diameter and 30 m in height. c) Three types of hydrometers (rimers, secondary ice particles, and drizzle drops) are identified based on their unique Doppler spectra fingerprints (detailed in the text). Five examples of actual Doppler spectra from our dataset containing different combinations of these particle classes are shown in Figure S6. d) The existence of rimers or drizzle drops in the neighborhood region of the central range gate containing secondary ice particles is used to determine whether the secondary ice event is caused by rime splintering or freezing fragmentation.

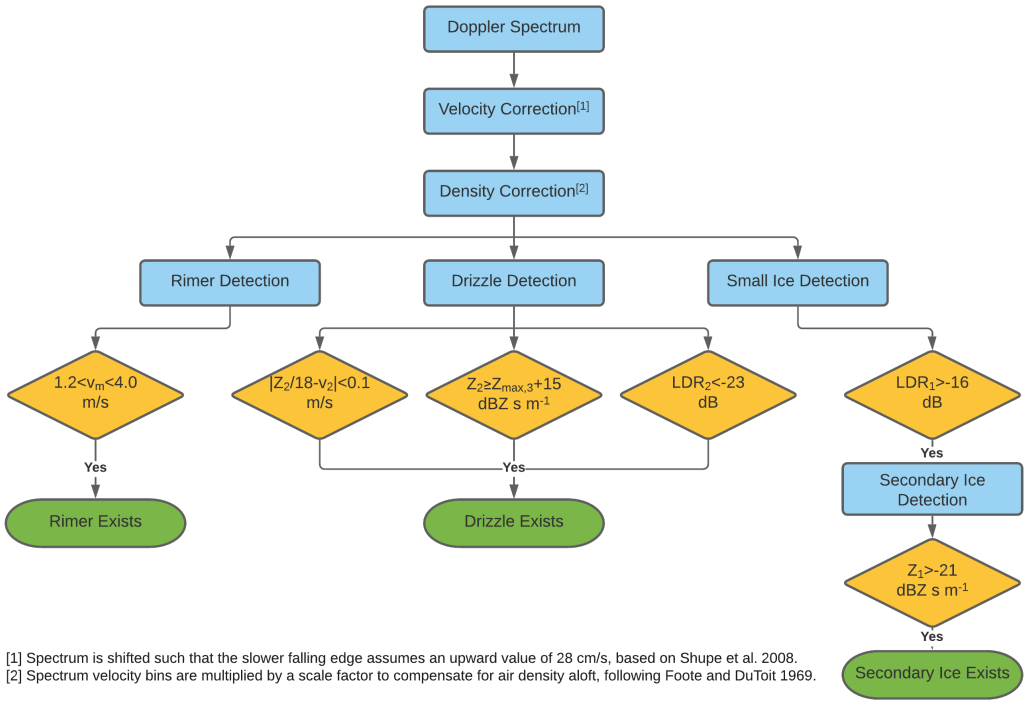

Fig. S5. A brief summary of identification of rimer, drizzle, and secondary ice particles. v_m is the modal spectrum velocity. Z is the spectral reflectivity and LDR is linear depolarization ratio. The subscript means different ranges of velocity bins: 1 is for velocities between 0 and 0.9 m s^{-1}, 2 is between 0 and 1.0 m s^{-1}, and 3 is between 1.15 and 1.3 m s^{-1}. For example, Z_2 means the spectral reflectivity for velocity bins between 0 and 1.0 m s^{-1}. Spectrum is shifted such that the slower falling edge assumes an upward value of 28 cm s^{-1} based on Shupe et al. 2008 (1). Spectrum velocity bins are multiplied by a scale factor to comprensate for air density aloft, following Foote and Du Toit 1969 (2).

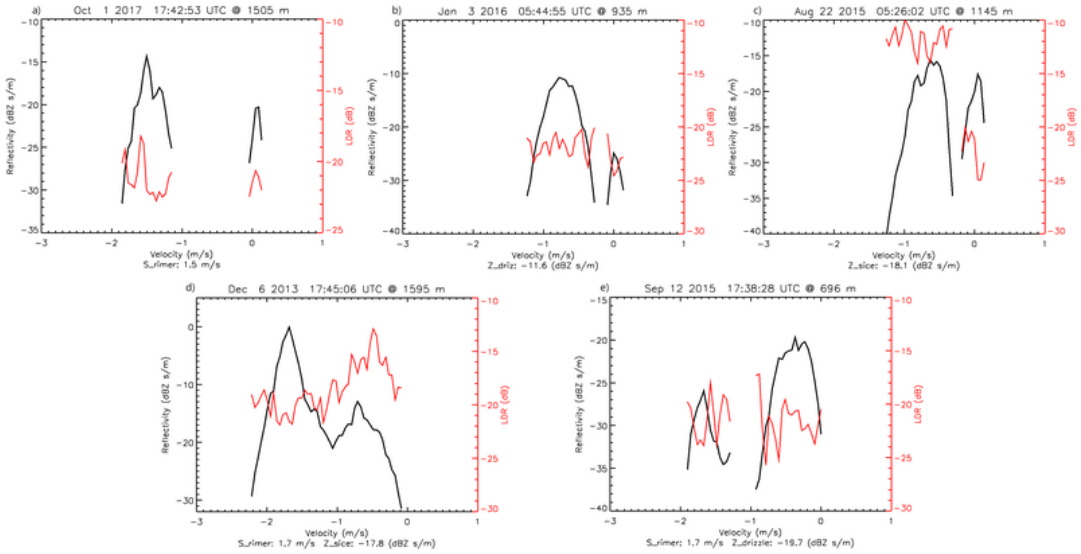

Fig. S6. Examples of Doppler spectra and LDR for rimer alone, drizzle alone, secondary ice alone, rimer plus secondary ice, and rimer plus drizzle. (a) Example of a Doppler spectrum containing the fingerprint of rimer alone. The rimer fall speed is 1.5 m s^{-1} at its modal reflectivity of -14 dBZ s m^{-1}. The small peak at 0 m s^{-1} with LDR less than -20 dB indicates spherical targets, which is consistent with and presumed to be cloud droplet echoes. (b) Example of a Doppler spectrum containing the fingerprint of drizzle alone. Detection relies on the relationship $|(-27.0 - Z_{driz})/18.0 - V_{driz}|<0.1$. Reflectivity peaks at -11.6 dBZ s m^{-1}, and LDR is less than -20 dB which indicates spherical particles. The small peak at 0 m s^{-1} with LDR less than -20 dB is consistent with, and presumed to be, cloud droplet echoes. (c) Example of a Doppler spectrum containing the fingerprint of secondary ice alone. Reflectivity peaks at -16 dBZ s m^{-1}, and LDR is greater than -15 dB indicates anisotropic, needle-like particles. The small peak at 0 m s^{-1} with LDR less than -20 dB is consistent with, and presumed to be, cloud droplet echoes. (d) Example of a Doppler spectrum containing the fingerprints of rimer and secondary ice in the same radar sampling volume. The rimer fall speed is 1.7 m s^{-1} at its modal reflectivity of 0 dBZ s m^{-1}, while the secondary ice has a reflectivity of -17.8 dBZ s m^{-1} where the LDR exceeds -15 dB, indicating needle-like particles. (e) Example of a Doppler spectrum containing the fingerprints of rimer and drizzle in the same sampling volume. The rimer fall speed is 1.7 m s^{-1} at its modal reflectivity of -25.5 dBZ s m^{-1}, while the drizzle has a peak reflectivity of -19.7 dBZ s m^{-1} with an LDR predominantly below -20 dB, indicating spherical particles.

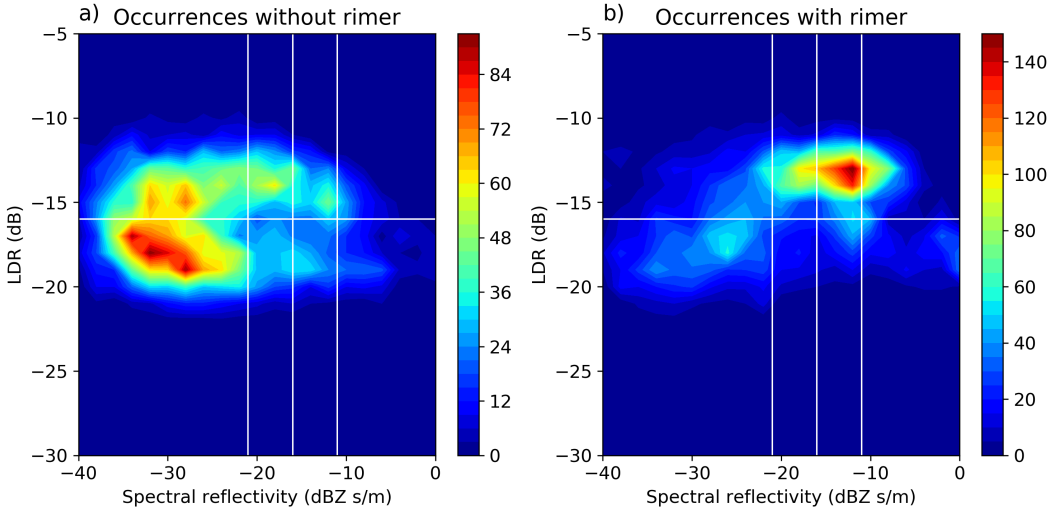

Fig. S7. Occurrence contour plots of slowly falling particles (10 to 90 cm s^{-1}) at -5 $\pm$ 1^{o}C as a function of their reflectivity and LDR a) without rimers and b) with rimers. The horizontal white line is the LDR threshold (-16 dB) for small ice particles, and the vertical white lines are different reflectivity thresholds (-21 dBZ s m^{-1}, -16 dBZ s m^{-1}, and -11 dBZ s m^{-1}) that are used for SIP event detection with increasing confidence (from left to right).

Table S1. Relationship between drizzle reflectivity, terminal fall speed, and drop diameter (and its uncertainty). The drop diameter uncertainty is inferred from the uncertainty in particle fall velocity of about 15 cm s^{-1}.

Drizzle reflectivity (dBZ s m^{-1})	Terminal fall speed (cm s^{-1})	Drop diameter and uncertainty (μm)
-25	11	63 ($\pm$ 51)
-24	16	79 ($\pm$ 46)
-23	22	93 ($\pm$ 40)
-22	27	107 ($\pm$ 37)
-21	33	120 ($\pm$ 35)
-20	38	132 ($\pm$ 35)
-19	44	145 ($\pm$ 33)
-18	50	157 ($\pm$ 33)
-17	55	169 ($\pm$ 33)
-16	61	182 ($\pm$ 33)
-15	67	194 ($\pm$ 33)
-14	72	206 ($\pm$ 33)
-13	78	218 ($\pm$ 33)
-12	83	230 ($\pm$ 33)
-11	89	243 ($\pm$ 33)
-10	94	255 ($\pm$ 33)
-9	100	267 ($\pm$ 33)
-8	106	279 ($\pm$ 33)
-7	111	292 ($\pm$ 33)
-6	117	304 ($\pm$ 33)
-5	122	317 ($\pm$ 33)

Movie S1. Needles recorded by the MASC at the North Slope of Alaska Atmospheric Radiation Measurement site on May 11, 2019 at around 11 UTC.

References

1. MD Shupe, P Kollias, M Poellot, E Eloranta, On deriving vertical air motions from cloud radar doppler spectra. *J. Atmospheric Ocean. Technol.* **25**, 547–557 (2008).
2. GB Foote, P Du Toit, Terminal velocity of raindrops aloft. *J. Appl. Meteorol.* **8**, 249–253 (1969).